JOURNAL OF QUATERNARY SCIENCE (2021) **36**(4) 570–585 ISSN 0267-8179. DOI: 10.1002/jqs.3317

JQS Journal of Quaternary Science QRA Quaternary Research Association

The Oyambre coastal terrace: a detailed sedimentary record of the Last Interglacial Stage in northern Iberia (Cantabrian coast, Spain)

ELISA SAINZ DE MURIETA,* PEDRO P. CUNHA,[2] ALEJANDRO CEARRETA,[1,3] ANDREW S. MURRAY[4] and JAN-PIETER BUYLAERT[5]

[1]Basque Centre for Climate Change (BC3), Edificio Sede 1, Bº Sarriena s/n, Leioa, Basque Country, Spain
[2]University of Coimbra, MARE - Marine and Environmental Sciences Centre, Department of Earth Sciences, Univ. Coimbra - Pólo II, Coimbra, Portugal
[3]Departamento de Geología, Facultad de Ciência y Tecnología, Universidad del País Vasco UPV/EHU, Bilbao, Spain
[4]Nordic Laboratory for Luminescence Dating, Department of Geoscience, Aarhus University, DTU Risø Campus, Roskilde, Denmark
[5]Department of Physics, Technical University of Denmark, DTU Risø Campus, Roskilde, Denmark

Received 31 March 2020; Revised 13 March 2021; Accepted 15 March 2021

ABSTRACT: A detailed study is presented of a 15.3-m-thick Pleistocene coastal terrace located on the Cantabrian coast (northern Spain). Stratigraphic, sedimentological, topographic and micropalaeontological information is combined with a chronology based on luminescence dating to characterize the deposits. The sedimentary succession records: (i) a basal transgressive system, consisting of a wave-cut surface covered by a lower layer of beach gravels and upper beach pebbly sands; and (ii) a thicker upper highstand system (aggrading), comprising medium to very fine aeolian sands interbedded with thin palustrine muds. Luminescence dating involved a detailed sampling strategy (36 samples and two modern analogues) and the use of both quartz optically stimulated luminescence (OSL) and feldspar post-infrared infrared stimulated luminescence single aliquot regeneration protocols; feldspar results were used to confirm the completeness of bleaching of the quartz OSL signal. The quartz OSL luminescence age–depth relationship shows significant dispersion, but nevertheless two rapid phases of deposition can be clearly identified: one at ~130 ka [Marine Oxygen Isotope Stage (MIS) 5] and one at ~100 ka (MIS 5c). The top of the succession is dated to ~70 ka. The MIS 5e marine maximum flooding surface is identified at an elevation of 6.85 m above mean seal level. This elevation provides evidence of a regional sea-level highstand for this sector of the Cantabrian coast.

KEYWORDS: coastal terrace; Last Interglacial Stage (LIG); MIS 5 regional sea-level highstand; northern Iberia; OSL dating

Introduction

Among the multiple changes already triggered by global warming, sea-level rise (SLR) represents a serious risk for coastal areas around the world; these concentrate a great part of global population and socioeconomic infrastructures (Revi *et al.*, 2014). The Quaternary (the last 2.58 Ma) has been characterized by frequent and rapid changes in Earth's climate and one of the many consequences resulting from these is the variation in global sea levels through time. Many Earth system components, such as orbital parameters, radiative forcing, landmass topography or ocean circulation, were different in the past and thus direct analogies between past and future climate changes should be avoided (Oldfield, 2005; Yin and Berger, 2015). Nevertheless, past analogues do provide the insights required to improve our knowledge of natural climate variability and its driving mechanisms. Future climate change will result from the interaction between natural processes and human activities, and without a sound understanding of these natural processes, it will be very difficult to identify and quantify the anthropogenic contribution. Thus, a better understanding of these interactions will contribute to improvements in the process-based models currently used to estimate future projections (Edwards *et al.*, 2001; Gilford *et al.*, 2020). It is therefore not only useful, but necessary, to look at the past to fully comprehend how the undisturbed Earth system functioned before human forcing became significant (Loutre and Berger, 2003; Oldfield, 2005).

Particular attention has been paid to Marine Oxygen Isotope Stage (MIS) 11, when sea-level highstand peaked at 410 ka (Loutre and Berger, 2003; Tzedakis, 2010; Candy *et al.*, 2014) and MIS 5, the Last Interglacial, ~125 ka (Kukla *et al.*, 2002; Tzedakis, 2003). The Last Interglacial Stage (LIG), or MIS 5, is considered 'the most recent geological interval during which conditions were similar to the present interglacial' (Tzedakis, 2003). CO_2 concentration during the LIG was similar to pre-industrial levels but warming had a strong orbital forcing and because of this, the analogy with the late Holocene climate has been questioned (Loutre and Berger, 2003). However, and despite these qualifications, the warm climate of MIS 5 (together with that of MIS 9 and MIS 11) is similar to that resulting from 'the anthropogenic warming in terms of climate feedbacks at the regional scale' (Yin and Berger, 2015). Global mean temperatures during this stage were at least 2 °C higher than present (Rohling *et al.*, 2008), Greenland and West Antarctic ice sheets were reduced in size (Goelzer *et al.*, 2016), sea level was, most probably, more than 5 m above current mean level (Cuffey and Marshall, 2000; Hearty *et al.*, 2007; Masson-Delmotte *et al.*, 2013;

*Correspondence to: Elisa Sainz de Murieta, as above.
E-mail: elisa.sainzdemurieta@bc3research.org

Dutton *et al.*, 2015) and rates of sea-level rise could have reached 1.6 m per century (Rohling *et al.*, 2008).

Mean global temperatures and rates of sea-level rise during this stage are close to some of the IPCC projections for the end of this century. For instance, Kopp *et al.* (2013) estimate that it is likely (66–100% probability) that rates of sea-level rise during the LIG were between 3 and 7 mm a^{-1} and higher rates are considered unlikely. During the period 1993–2001, rates of around 3 mm a^{-1} have already been observed (Hay *et al.*, 2015) and by 2100 these could be 4–9 mm a^{-1}, under the most optimistic climate scenario (RCP2.6). In the most unfavourable scenario (RCP8.5), rates of sea-level rise could reach 15 mm a^{-1} (Oppenheimer *et al.*, 2019). Therefore, the MIS 5 interval has received increasing attention, particularly regarding changes in sea level. Shorelines developed during the MIS 5 highstand represent the best preserved and most geographically widespread record of a higher-than-present global mean sea level during a previous Quaternary interglacial (Dutton *et al.*, 2015).

Despite many advances in our understanding of global mean sea level during past interglacials, it is still necessary to improve the accuracy and precision of the age and elevation of relative sea-level (RSL) indicators (Dutton *et al.*, 2015). It is commonly accepted that the MIS 5 includes three RSL highstands: MIS 5e (130–116 ka), MIS 5c (~100 ka) and MIS 5a (~80 ka) (e.g. Stirling *et al.*, 1998; Murray-Wallace and Woodroffe, 2014; Creveling *et al.*, 2017), although the occurrence of rapid sea-level fluctuations within MIS 5e has been recently questioned (Barlow *et al.*, 2018).

Palaeoshorelines record the position of former high relative sea levels, the position of which is a result of a combination of eustatic, isostatic and tectonic process (Lambeck *et al.*, 2002). Raised platforms and marine terraces along the Cantabrian coast of northern Spain have been studied before to analyse sea levels and document uplift, but the presumed MIS 5 shoreline has never been accurately dated in this area (e.g. Alonso and Pagés, 2007; López-Fernández *et al.*, 2020). One of these terraces is located on the north-western side of the Oyambre beach and makes up part of the modern cliffs in this coastal area. These cliffs are mainly cut into soft lithologies of Oligocene age, and are retreating rapidly. Using aerial photographs, García-Codrón and Rasilla Álvarez (2006) calculated a coastline retreat in this area of 13–15 m between 1957 and 2001. The Oyambre Pleistocene terrace comprises a 15.3-m-thick coastal sequence made of gravels, sands and some muds, located on top of an erosive surface (wave-cut platform) at about 4.50 m above present Bilbao mean sea level (MSL), corresponding to 6.90 m above the Bilbao ordnance datum (Fig. 1). This angular discordance separates Oligocene sandy marls from a probable LIG/MIS 5 deposit. Mengaud (1920) was the first to mention the existence of this raised Quaternary deposit ('diluvium quaternaire') at Oyambre, and it was later described in some detail by Mary (1971) who assigned a Tyrrhenian age (Eemian, in Mary, 1983) to this marine deposit based on its topographic position. Flor (1980) described the outcrop as a sequence consisting of basal beach gravels and sands followed by aeolian dune sands with interbedded clays deposited by solifluction under cold climate conditions. Garzón *et al.* (1996) performed amino acid racemization analyses on two types of marine mollusc shells (*Cardium* and *Patella*) from the basal unit which showed discrepant ages of 72 ± 13 and 21 ± 9 ka, respectively; they considered that the first date was more acceptable for this raised-beach level. In 2010, we carried out an accelerator mass spectrometry (AMS) radiocarbon dating of a shell sample (Beta-287876) from the same basal layer of beach gravels and sands that gave an age of >43 500 a BP, beyond the resolution of this dating method. In addition, a recent comprehensive review on the elevated coastal platforms in this north Iberian margin performed by López-Fernández *et al.* (2020) concluded that the most recent Cantabrian marine terraces have not been tectonically uplifted and thus they must be explained by eustatic sea-level changes during pre-Holocene times. We deduce that, in the absence of identified neotectonic activity on this coastal area, the Oyambre coastal terrace is likely to record a eustatic Late Pleistocene highstand.

This study sets out to characterize the sedimentary succession of the Oyambre coastal terrace and to determine whether it indeed represents the MIS 5 sea-level highstand on the Cantabrian coast, or whether it is, in fact, older. This is

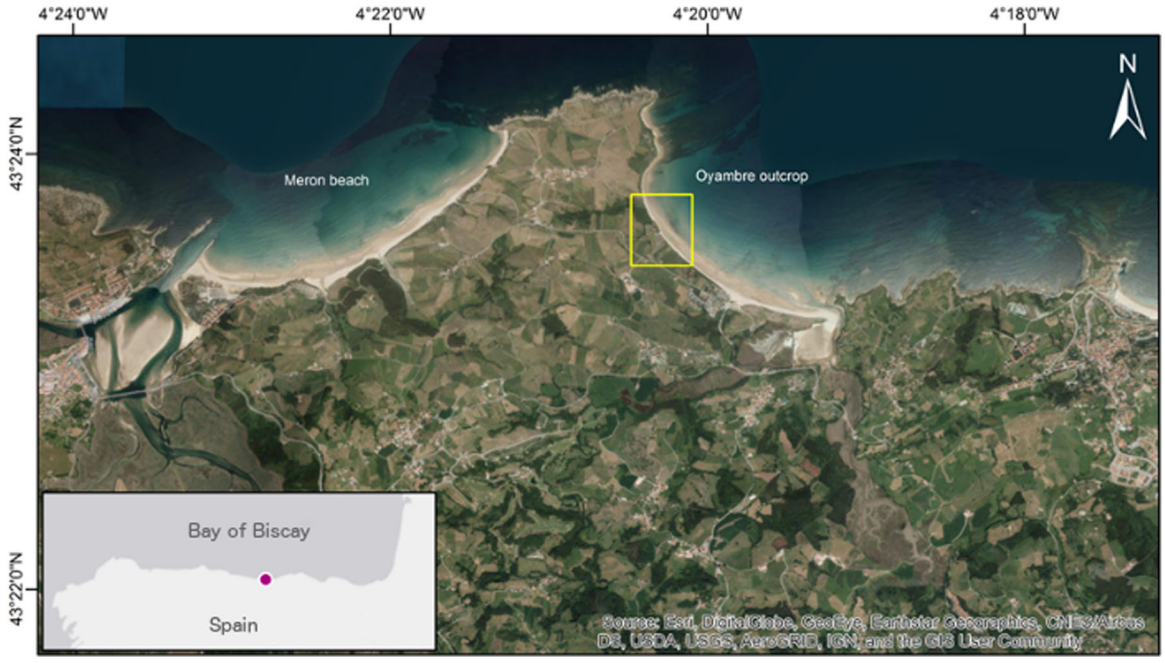

Figure 1. Location of the studied outcrop at Oyambre beach (Cantabrian coast, northern Spain), protected from the predominant NW waves. Satellite image from Esri Basemap Gallery. [Color figure can be viewed at wileyonlinelibrary.com]

achieved by employing luminescence dating to independently constrain the age of this Pleistocene sequence. This geological archive has not been corrected for glacial isostatic adjustment (GIA), and so represents an RSL record.

Materials and methods

Fieldwork

The coastal study site is located 5 km to the east of the village of San Vicente de la Barquera, in the western part of the Cantabria province (Fig. 2). Middle Eocene deposits outcrop at the Oyambre Cape, which consist of shallow-marine limestones (Colombres and Serdio formations) and Biarritzian marls (Acebosa Formation). Oligocene sandy marls (Meron Formation) outcrop to the east and west of the cape, in the Oyambre and Meron beaches, respectively (Fig. 2) (Payros *et al.*, 2015).

This study used a standard fieldwork approach involving topography, lithostratigraphy and sedimentology of the sedimentary succession.

Samples for luminescence dating were collected in May–June 2012 by hammering opaque steel tubes (7 × 30 cm) into the sediment (Fig. 3, left), after the outcrop had been cleaned by excavating ~0.5 m from the original surface. Starting from the top of the basal boulder gravel layer 1, 36 samples were collected, up to the topmost terrace deposits (Ploy-01 to Ploy-36). Two very young/modern sediment samples were also collected, one from the Oyambre beach (Ploy-00) and the other from aeolian sands of the nearby active dune (Ploy-dune), as modern analogues for optically stimulated luminescence (OSL) dating. Each light-protected sample was accompanied by 350–500 g of sediment (additional bag) collected immediately adjacent to each sampling tube (Fig. 3, right); separate subsamples of this material were used for grain size analysis, microfossil counting, water content determination (field and in saturation) and dose rate measurement (Sainz de Murieta, 2016). In all cases, the sampled sediment was coarse to fine sand or silty clay, with a high concentration of felsic minerals: quartz (predominant), feldspars and muscovite. The detailed sampling strategy allowed us to collect material from each significant sedimentary layer, up to three samples per level, depending on the unit thickness (e.g. Cunha *et al.*, 2008).

The precise location and elevation of sedimentary layers, tubes and surface samples were determined by using a Global Positioning System-Real Time Kinematic (GPS-RTK) and a total station, with a horizontal precision of ±2 cm and a vertical accuracy of ±3.5 cm. Coordinates *x*, *y* and *z* of the samples are referred to the ED50 geographical system in planimetry and the Bilbao ordnance datum, which is 2.40 m below Bilbao MSL. The precise geographical and topographic position of the samples (tubes) is shown in Table S1 (Supporting Information).

Grain size and compositional analysis of the sediment

Sediment textural and compositional analyses were performed at the Sedimentology Laboratory of the Department of Earth Sciences – University of Coimbra. The grain size distribution of each sediment sample of sand or silty-clay was determined by laser diffraction analysis, using a Beckman Coulter LS230 laser granulometer (0.4–2000 μm). The volume statistics (mean, median, standard deviation, skewness and kurtosis) were obtained by the geometric method of moments. The modes and the percentages of sand (2000–63 μm), silt (63–4 μm) and clay (<4 μm) fractions were also determined.

The mineralogical composition of the sand fraction was obtained by observation using a Wild mod. Heerbrugg 84220 stereoscopic binocular microscope (50×). The mineralogical composition of the <2-μm fraction was determined by X-ray diffraction of orientated samples, before and after treatment with ethylene glycol and heating to 550 °C. A Philips PW 3710 X-ray diffractometer with a Cu tube (at 40 kV and 20 nA) and software package APD 3.6J-Automatic Powder Diffraction (Philips) were used.

Foraminiferal analysis

Benthic foraminiferal content was analysed in one sample from the basal boulder gravel layer 1 (Oyambre 1), in the 36

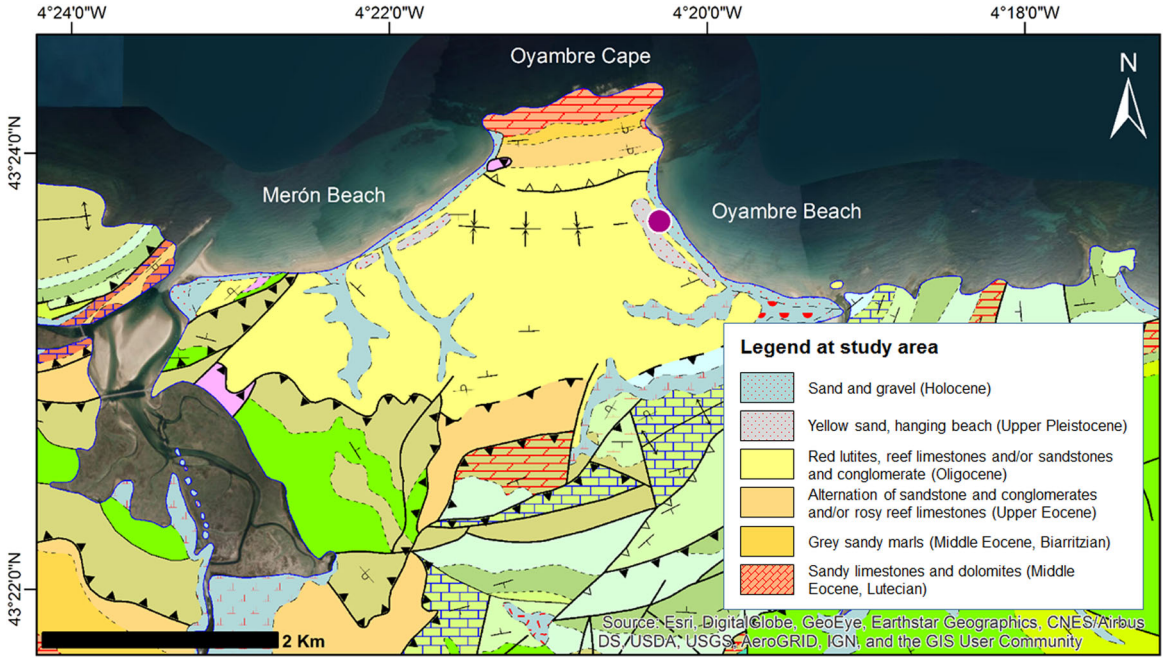

Figure 2. Geological map of western Cantabria (north Spain), including Oyambre beach (red dot), located east of Oyambre Cape. Source: geological map of the Spanish Geology and Mining Institute (IGME). [Color figure can be viewed at wileyonlinelibrary.com]

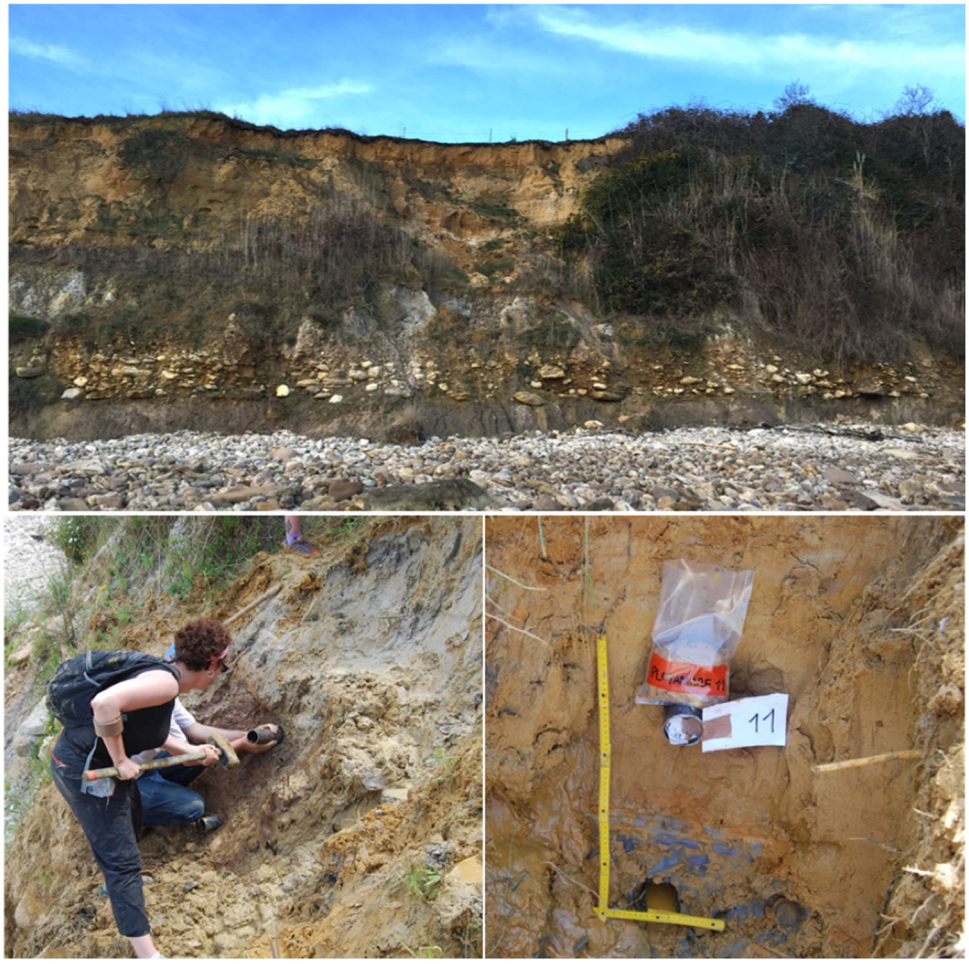

Figure 3. View of the Oyambre outcrop (upper picture) and sampling procedure. Left: metal tubes were introduced into the sediment using a hammer. Right: sample Ploy-11 was obtained by the insertion of a steel tube into the sandy sediment and also collecting extra bags with an adjacent sub-sample. The lower sample (Ploy-10) was collected from a dark, very fine silt layer. [Color figure can be viewed at wileyonlinelibrary.com]

samples collected above up to the topmost terrace deposits (Ploy-01 to Ploy-36) and in one sample from the modern Oyambre beach (Ploy-00). The sampling interval reflects our interest in characterizing the depositional environment of each of the layers from which light-protected samples were taken for OSL dating. These 38 samples were wet sieved through 2-mm and 63-μm sieves to remove large and fine-grained sediments, respectively, at the Micropalaeontology Laboratory of the UPV/EHU. Sand-sized material (retained in the 63-μm sieve) was oven dried at 60 °C and weighed. Foraminifera were concentrated by flotation in trichloroethylene as described by Murray (1979). To ensure statistical representativeness of foraminifera counting, when possible, a minimum of 300 tests per sample were extracted. Otherwise, when the statistical minimum was not reached, all tests present were identified. The micropalaeontological study was carried out using a Nikon SMZ 645 stereoscopic binocular microscope, with reflected light.

Luminescence dating

Quartz (Qtz) sedimentary grains from the Oyambre terrace deposits were used as dosimeters for the OSL dating of this sedimentary sequence. The rationale behind luminescence methods relies on a particular property of many minerals, quartz and feldspars among them; they are able to store energy within their crystal structures (e.g. Duller, 2008). Some of this energy is released in the form of light when subjected to different stimuli, such as heat or (day)light; this light from the mineral is called luminescence (Aitken, 1998). If other environmental parameters remain stable, luminescence will increase with time from the date in which it was buried, until the crystal is unable to store more energy. OSL dating techniques play a key role in establishing absolute dates for Holocene to Middle Pleistocene sediments. Quartz OSL dating usually has an upper dating limit in the range 100–200 ka (e.g. Murray and Funder, 2003; Buylaert *et al.*, 2012), whereas radiocarbon dating is limited to the last ~45 ka and requires *in situ* organic matter of the same age as the depositional event. With to the development of the single aliquot regeneration (SAR) procedure (Murray and Wintle, 2003; Wintle and Murray, 2000), quartz has become the preferred dosimeter to date sandy sediments of LIG age (e.g. Murray and Funder, 2003; Murray *et al.*, 2007; Lamothe, 2016).

For OSL dating, sediment samples were processed using conventional methods (Aitken, 1998). The preparation of the OSL mineral fractions from the inner parts of the tubes was carried out in the sample preparation room of the Department of Earth Sciences – University of Coimbra, under subdued red light to prevent resetting of the luminescence signal. Each sample was wet sieved to separate the 180–250-μm grain size fraction. This fraction was then treated with 10% HCl to remove carbonates, followed by 10% H_2O_2 to remove reactive organic matter. The K-feldspar-rich fraction was separated by floating in heavy liquid (sodium polytungstate solution; $\rho = 2.58\ g\ cm^{-3}$). Floating grains were then etched using 10% HF acid for 40 min to dissolve the alpha-irradiated surface layer, and to remove surface weathering and coatings. Any

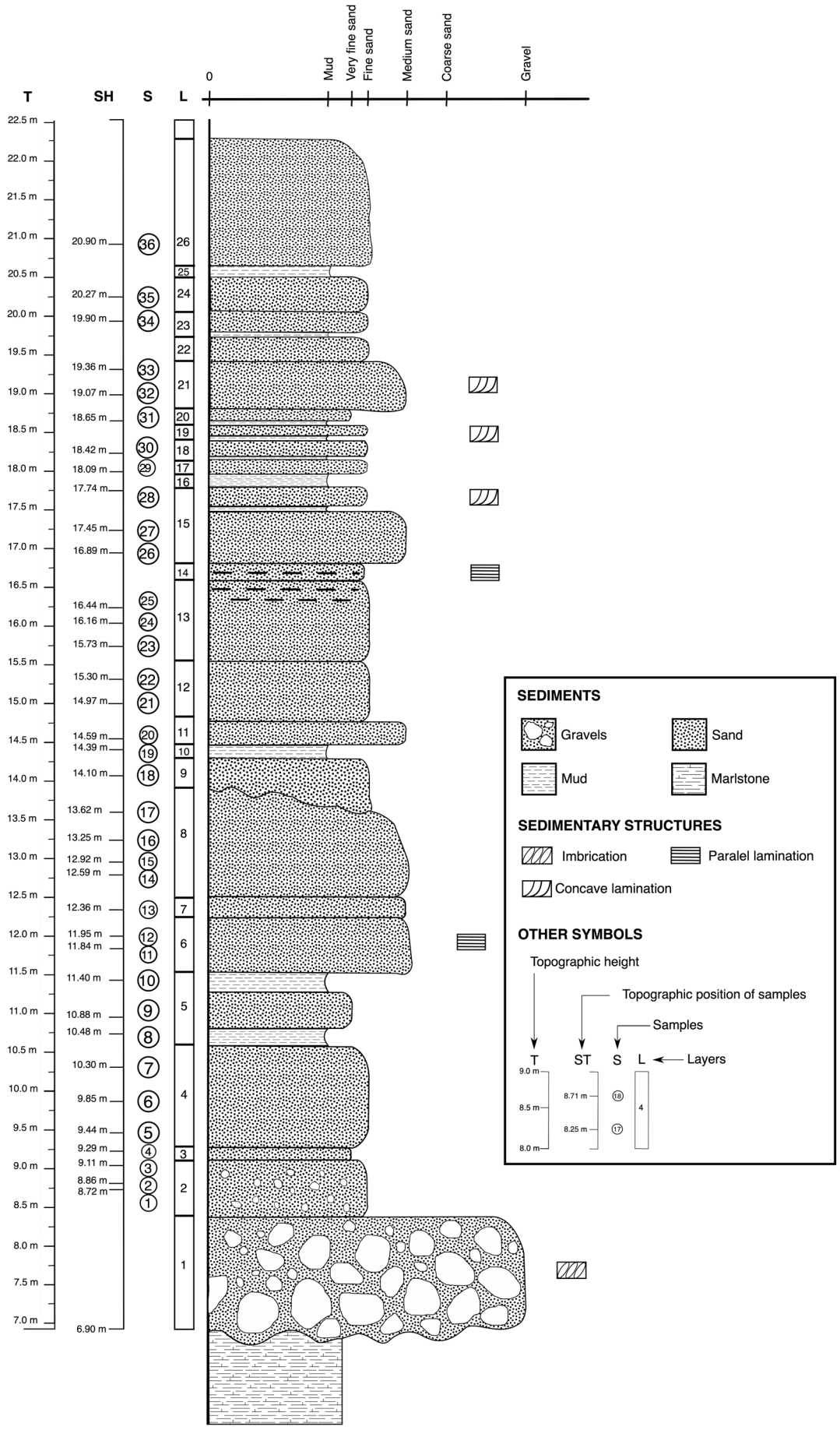

Figure 4. Stratigraphic log of the Oyambre terrace succession (15.3 m; vertical scale in metres). T – elevation (above Bilbao ordnance datum – a.B.o.d.); SH – elevation of samples (a.B.o.d.); S – location of the samples in the stratigraphy; L – sedimentary layers. The base of the terrace is at 6.90 m a.B.o.d., corresponding to 4.5 m above present mean sea level (MSL).

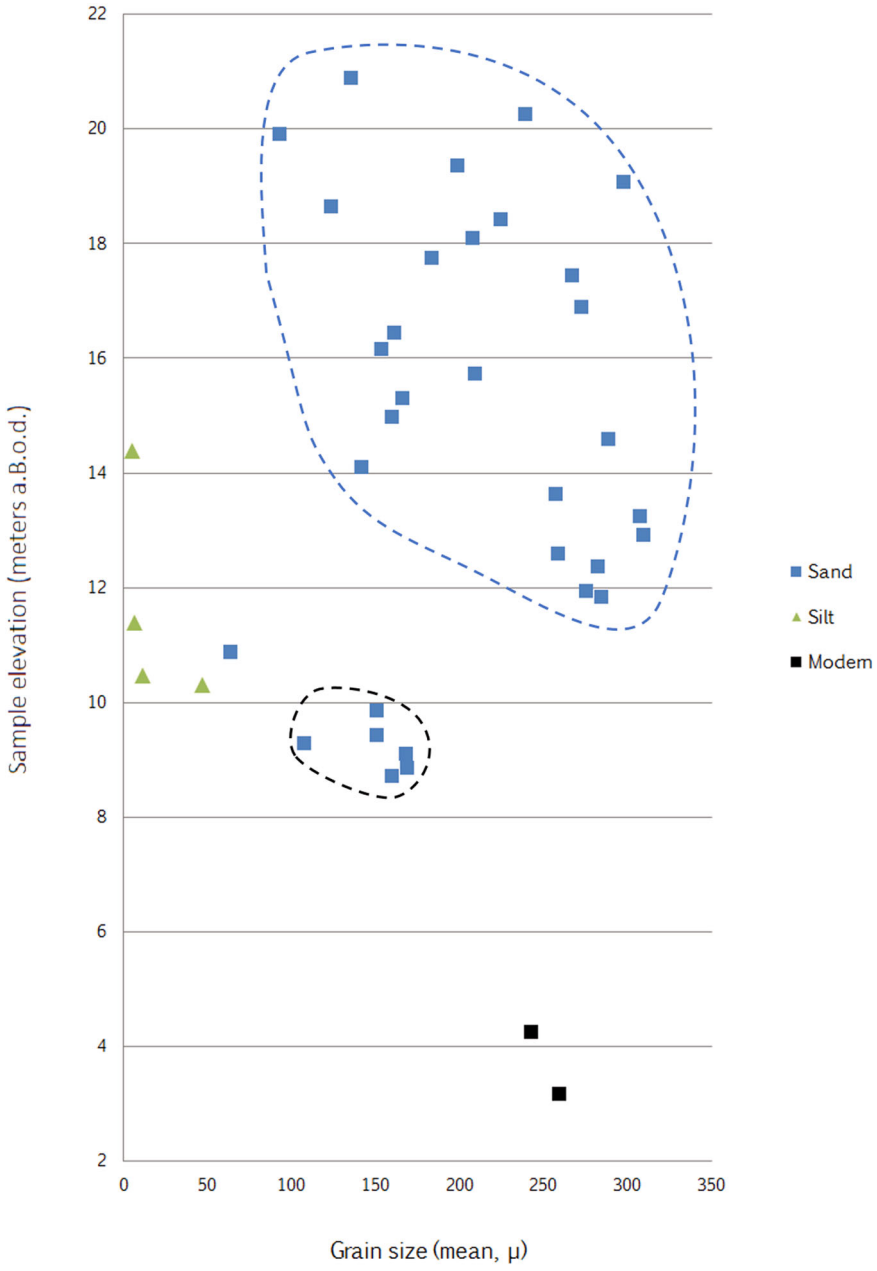

Figure 5. Mean sediment grain-size plotted versus sample elevation (above Bilbao ordnance datum). [Color figure can be viewed at wileyonlinelibrary.com]

fluoride contamination was then removed using a 10% HCl solution for 20 min. A similar treatment was applied to the fraction $\rho > 2.58\ g\ cm^{-3}$ to obtain quartz grains but using concentrated (40%) HF for 60 min followed by 10% HCl for 40 min in the final two stages (e.g. Cunha *et al.*, 2019).

Radionuclide concentrations (^{238}U, ^{232}Th and ^{40}K) in the bulk sediment were measured using high-resolution gamma spectrometry. The additional sediment sample associated with the main OSL sample was first dried at 50 °C, a subsample of ~250 g was pulverized and homogenized, and then heated to 450 °C for 24 h to remove any organic matter (weight loss recorded). Finally, this material was cast in wax to prevent radon loss and to provide a reproducible counting geometry. Samples were stored for 3 weeks to allow ^{222}Rn to reach equilibrium with its parent ^{226}Ra before being measured on a high-purity germanium detector for at least 24 h. Details on the gamma spectrometry calibration are given in Murray *et al.* (2018). The external beta and gamma dose rate is the same for both quartz and K-feldspar grains. For quartz, a small internal dose rate of $0.02 \pm 0.01\ Gy\ ka^{-1}$ was assumed (Vandenberghe *et al.*, 2008). For K-feldspar grains an internal beta dose rate due to internal K (and Rb) of $0.839 \pm 0.041\ Gy\ ka^{-1}$ was used based on X-ray fluorescence (XRF) measurements of the K-feldspar extracts [average K concentration = $12.2 \pm 0.3\%$ ($n = 17$)]. For K-feldspar an internal dose rate from U, Th of $0.10 \pm 0.05\ Gy\ ka^{-1}$ was assumed. The radionuclide concentrations were converted to dose rate data using the conversion factors from Guérin *et al.* (2011). The contribution from cosmic radiation to the dose rate was calculated following Prescott and Hutton (1994) assuming an uncertainty of 5%. The long-term water content of each sample was estimated based on the average of the field water content and saturation water content. Equivalent doses were obtained on Risø TL/OSL DA-20 readers. Quartz grains were mounted as large (8 mm) aliquots on stainless steel discs or cups. Feldspar grains were mounted as medium (~4 mm) aliquots on stainless steel cups.

A standard SAR protocol was used to estimate the quartz D_e (Wintle and Murray, 2000; Murray and Wintle, 2003). The blue (470 ± 30 nm) stimulated OSL signal was detected through a U-340 filter. All samples had a strong fast component. The net OSL signal was calculated from the initial 0.0–0.32 s of stimulation and an early background between 0.32 and 0.64 s. Feldspar D_e values were measured using a post-infrared infrared stimulated luminescence $(pIRIR)_{200,290}$

Table 1. Results of the grain size analysis of the samples obtained at the Oyambre outcrop.

NLL lab code	Field code	Layer	Mean (μm)	Mean	Median (μm)	Modes (μm)	SD	Skew		Kurtosis		Sand (%)	Silt (%)	Clay (%)
122294	Ploy-36	26	135.3	Fine sand	215.9	295.5; 50	3.569	−1.393	Left skewed	2.213	Leptokurtic	75.28	22.39	2.33
122293	Ploy-35	24	239.5	Fine sand	305.2	324.4; 40	2.849	−2.649	Left skewed	8.398	Leptokurtic	90.71	7.91	1.08
122292	Ploy-34	23	92.5	Very fine sand	244.7	295.5; 6; 50	6.898	−1.032	Left skewed	−0.383	Platykurtic	69.85	19.14	11.00
122291	Ploy-33	21	198.5	Fine sand	271	295.5; 45	2.973	−2.252	Left skewed	6.112	Leptokurtic	87.40	11.10	1.50
122290	Ploy-32	21	297.4	Medium sand	324.7	324.4	2.077	−3.69	Left skewed	21.140	Leptokurtic	96.50	2.88	0.62
122289	Ploy-31	20	123.7	Very fine sand	207.7	269.2; 40	3.816	−1.254	Left skewed	1.652	Leptokurtic	71.80	25.58	2.62
122288	Ploy-30	18	224.4	Fine sand	273.5	295.5	2.552	−2.658	Left skewed	9.913	Leptokurtic	91.67	7.27	1.06
122287	Ploy-29	17	208.1	Fine sand	267.6	295.5	2.769	−2.449	Left skewed	7.912	Leptokurtic	90.13	8.58	1.29
122286	Ploy-28	15	183.7	Fine sand	262.7	295.5; 50	3.025	−2.189	Left skewed	5.454	Leptokurtic	85.54	12.89	1.57
122285	Ploy-27	15	266.7	Medium sand	333.1	324.4	3.069	−3.215	Left skewed	11.150	Leptokurtic	94.23	3.39	2.38
122284	Ploy-26	15	272.8	Medium sand	331.4	324.4	2.894	−3.555	Left skewed	14.310	Leptokurtic	94.46	3.24	2.30
122283	Ploy-25	13	161.3	Fine sand	282.4	324.4	4.736	−1.843	Left skewed	2.614	Leptokurtic	82.59	11.59	5.82
122282	Ploy-24	13	153.7	Fine sand	306.7	356.1; 8	5.441	−1.567	Left skewed	1.306	Leptokurtic	79.27	14.33	6.40
122281	Ploy-23	13	209.4	Fine sand	323.2	324.4	4.166	−2.255	Left skewed	4.504	Leptokurtic	87.18	8.61	4.21
122280	Ploy-22	12	166	Fine sand	302.6	324.4; 10	4.894	−1.691	Left skewed	1.925	Leptokurtic	81.59	13.19	5.22
122279	Ploy-21	12	159.7	Fine sand	310.4	356.1; 10	5.330	−1.665	Left skewed	1.579	Leptokurtic	80.28	13.48	6.23
122278	Ploy-20	11	288.8	Medium sand	356.5	356.1	2.950	−3.223	Left skewed	11.970	Leptokurtic	92.25	5.22	2.53
122277	Ploy-19	10	5.3	Very fine silt	5.7	9.371; 50	2.898	−0.032	Left skewed	−0.479	Platykurtic	0.18	60.82	39.00
122276	Ploy-18	9	141.8	Fine sand	300	356.1; 8	5.908	−1.522	Left skewed	1.025	Leptokurtic	79.54	12.71	7.75
122275	Ploy-17	8	257.1	Medium sand	337	324.4	3.533	−2.766	Left skewed	8.114	Leptokurtic	91.05	5.50	3.45
122274	Ploy-16	8	307.6	Medium sand	339.4	324.4	2.430	−3.939	Left skewed	20.330	Leptokurtic	95.15	2.92	1.93
122273	Ploy-15	8	309.4	Medium sand	360.3	356.1	2.707	−3659	Left skewed	16.200	Leptokurtic	95.39	2.81	1.80
122272	Ploy-14	8	259	Medium sand	332.3	324.4	3.136	−3.221	Left skewed	11.260	Leptokurtic	92.37	4.58	3.05
122271	Ploy-13	7	282.7	Medium sand	313.8	324.4	2.276	−4.028	Left skewed	22.730	Leptokurtic	96.70	2.16	1.14
122270	Ploy-12	6	275.6	Medium sand	324.3	324.4	2.698	−4.015	Left skewed	18.220	Leptokurtic	1.99	2.09	95.92
122269	Ploy-11	6	284.4	Medium sand	330.7	324.4	2.593	−4.193	Left skewed	20.340	Leptokurtic	96.46	1.71	1.83
122268	Ploy-10	5	6.4	Very fine silt	7	10.3	2.813	−0.192	Left skewed	−0.419	Platykurtic	0.17	68.22	31.61
122267	Ploy-09	5	63.6	Very fine sand	98.7	223.4; 50; 10	4.806	−0.901	Left skewed	0.192	Leptokurtic	59.91	32.94	7.15
122266	Ploy-08	5	11.6	Fine silt	12	12.40; 40; 150	3.804	−0.112	Left skewed	0.499	Platykurtic	10.98	67.39	21.63
122265	Ploy-07	4	46.8	Coarse silt	78.5	269.2; 10; 50	6.587	−0.581	Left skewed	0.876	Platykurtic	52.33	34.00	13.67
122264	Ploy-06	4	150.4	Fine sand	264.3	295.5	4.500	−1.895	Left skewed	2.796	Leptokurtic	81.93	12.92	5.15
122263	Ploy-05	4	150.4	Fine sand	267.9	295.5	4.843	−1.741	Left skewed	2.241	Leptokurtic	81.00	13.08	5.92
122262	Ploy-04	3	107.7	Very fine sand	216.2	245.2; 50; 8	5.874	−1.428	Left skewed	0.903	Leptokurtic	77.53	13.12	9.35
122261	Ploy-03	2	168.4	Fine sand	226.8	245.2	3.671	−2.156	Left skewed	5.315	Leptokurtic	88.27	7.90	3.83
122260	Ploy-02	2	168.9	Fine sand	230.1	245.2	3.527	−2.236	Left skewed	5.745	Leptokurtic	88.43	8.26	3.31
122259	Ploy-01	2	159.5	Fine sand	228.5	245.2	3.695	−2.161	Left skewed	4.899	Leptokurtic	86.71	9.37	3.92
122258	Ploy-dune	Aeolian dune	242.3	Fine sand	238.1	245.2	1.360	0.851	Right skewed	2.137	Leptokurtic	100.00	0.00	0.00
122257	Ploy-00	Beach	259.7	Medium sand	254	245.2	1.438	0.47	Right skewed	0.921	Leptokurtic	100.00	0.00	0.00

Table 2. Results of the mineralogical analysis by X-ray diffraction of the <2-μm fraction of four silt samples from the Oyambre terrace succession.

Sample field code	Mixed layers I–V (%)	Chlorite (%)	Smectite (%)	Vermiculite (%)	Illite (%)	Kaolinite (%)	Clay mineral association	Other minerals
Ploy-25	28	0	0	60	7	5	V mix-I–V i k	Quartz
Ploy-19	0	0	12	60	20	8	V i s k	Quartz
Ploy-10	0	0	0	73	18	9	V i k	Quartz
Ploy-08	0	10	0	60	18	12	V i k c	Quartz, K-feldspar

protocol and the results calculated as in Stevens *et al*. (2018). Dividing the D_e by the environmental dose rate (in Gy ka^{-1}) gives the luminescence age of the sediment.

Results

Characterization of the sedimentary succession

At the Oyambre outcrop, located topographically above modern beach deposits, the Pleistocene coastal terrace onlaps a palaeowave-cut surface (at an elevation of 6.85 m above Bilbao ordnance datum – a.B.o.d.; 4.50 m above MSL) eroded into soft Oligocene sandy marls. The sedimentary succession of the terrace (15.30 m in total) comprises two lithostratigraphic units, subdivided into 26 horizontal layers (Fig. 4).

The lower unit (2.26 m thick; layers 1–3) includes: a basal layer 1 of boulder gravels, with imbrication and 1.50 m thick (located from 6.85 to 8.42 m a.B.o.d.) containing some bioclasts and foraminiferal assemblages, both indicative of a beach environment (see Microfossil analysis below), followed by yellow–brown pebbly fine sands (0.83 m thick, from 8.42 to 9.25 m a.B.o.d.) (layers 2 and 3).

The second unit comprises the upper 13.04 m of the succession (9.25–22.29 m a.B.o.d.) and consists of layers of medium to fine sands intercalated with usually thinner mud layers (layers 4–26). We find white–grey fine sands at the base (layer 4), followed by layer 5 which comprises a grey mud at the base, then of grey sandy mud, and black mud at the top. Layer 6 consists of laminated yellow medium sand, followed by massive white sand (layer 7) and then massive yellow medium sand (layer 8). Layer 9 has an erosive surface at the base and comprises brown medium sands. At its top, we find a layer (10) of very fine grey silt, followed by white medium sand (layer 11) and then yellow and grey fine sands (layers 12 and 13). Laminated brown medium muddy sand is found next (layer 14), followed by yellow to beige medium sands, alternating with dark clays (layers 15–20). Medium white sands with cross-bedding grade upwards to muddy fine and very fine sands (layers 21–23). The succession culminates with a beige medium sand (layer 24), a thin intercalation of a grey muddy sand (layer 25) and a topmost layer of yellow medium to fine sand (layer 26).

Grain size and mineralogical analysis

The results of grain size analysis of samples collected from the terrace deposit are presented Fig. 5 and Table 1. Note that for the grain size analysis of the samples Ploy-1, 2 and 3 (collected from layer 2), the few dispersed pebbles were not considered. The mineralogy of the fraction <2 μm, obtained from four silt samples, documents a predominance of vermiculite, associated with illite and kaolinite (Table 2). Probably, most of the clay minerals were sourced from erosion of the Oligocene marls exposed on the palaeocliff. The occurrence of smectite in sample Ploy-19 points to mineral transformation (vermiculite to smectite) in a poorly drained, wet environment, under temperate climate conditions.

Considering the analytical and field data, it is possible to identify two depositional environments in the sedimentary succession. The first is formed by the gravels and the brown fine sands with well-rounded pebbles of unit 1 (layers 1–3), representing an ancient beach environment. The maximum flooding surface (maximum sea-level highstand above the Bilbao ordnance datum) is represented by the boundary between layers 3 and 4, i.e. between the top of unit 1 (the youngest beach deposits) and unit 2. Based on its stratigraphic position, sedimentological features and the results of the grain size analysis (well-sorted fine sands) presented in Tables 1 and 2, the second part of the succession (unit 2), which comprises yellow or white–grey medium to fine sands that alternate with grey to dark muds, is interpreted as representing aeolian sands interbedded with thin palustrine organic muds (layers 4–26). Field observations and laboratory characterization indicate that the palaeoenvironments recorded by the terrace deposits are very similar to the modern ones near the Oyambre beach (Fig. 1). The terrace sedimentary succession, which discordantly overlays the substratum, records an initial transgressive evolution corresponding to the basal gravelly beach environment (MIS 5e or remnant old beach), followed by regressive evolution (coastal aggradation) evidenced by the transition from upper beach sands to the aeolian and palustrine deposits.

Microfossil analysis

Samples Ploy-00 and Oyambre 1 contain very abundant foraminiferal assemblages (Table 3). More than 300 tests were counted in sample Ploy-00 collected from the modern beach environment. Seventeen marine taxa were identified, with *Cibicidoides lobatulus* as the dominant species of the assemblage (79%) followed by *Rosalina anomala* (7%) and *Massilina secans* (4%). Other taxa were represented by one to three tests only. An abundant foraminiferal assemblage was also obtained in sample Oyambre 1 collected from the basal boulder gravel layer 1, which corresponds to the palaeobeach environment. Planktonic foraminifera were very abundant (approximately 40%) and Oligocene benthic species were also found together with Quaternary marine taxa (32 species) dominated by *Cassidulina obtusa* (15%), *Cibicidoides lobatulus* (14%), *Brizalina* spp. (14%), *Gavelinopsis praegeri* (9%) and *Bolivina pseudoplicata* (5%).

By contrast, fthe oraminiferal content of samples Ploy-01 to -36 was extremely low (Table 3). Only 23 tests were found in all. Most samples were barren of foraminifera and only eight samples contained very scarce microfossils (counts 1–12). *Trochammina inflata*, *Entzia macrescens*, *Arenoparrella mexicana*, *Ammonia tepida*, *Cribroelphidium excavatum* and *Bulimina gibba* are the only foraminiferal species present in these samples. Considering the sedimentological characterization and grain size analysis, we interpret these sandy materials in unit 2 to be of probable aeolian origin and the extremely low content of foraminifera supports this palaeoenvironmental interpretation.

Table 3. Summary of benthic foraminiferal results from the Oyambre samples.

	Absolute numbers of main benthic foraminiferal species													Parameters						
Sample	*Arenoparrella mexicana*	*Entzia macrescens*	*Trochammina inflata*	*Massilina secns*	*Ammonia tepida*	*Bolivina pseudoplicata*	*Brizalina spp.*	*Bulimina gibba*	*Cassidulina obtusa*	*Cibicidoides lobatulus*	*Cribroelphidium excavatum*	*Gavelinopsis praegeri*	*Rosalina anomala*	No. of tests	No. of species	% Open marine tests	% Marginal marine tests	% Agglutinated tests	% Porcellaneous tests	% Hyaline tests
Ploy-36														0	0	–	–	–	–	–
Ploy-35		1	2											3	2	–	–	–	–	–
Ploy-34														0	0	–	–	–	–	–
Ploy-33														0	0	–	–	–	–	–
Ploy-32	2		9		1									12	3	–	–	–	–	–
Ploy-31														0	0	–	–	–	–	–
Ploy-30								1						1	1	–	–	–	–	–
Ploy-29														0	0	–	–	–	–	–
Ploy-28														0	0	–	–	–	–	–
Ploy-27														0	0	–	–	–	–	–
Ploy-26														0	0	–	–	–	–	–
Ploy-25														0	0	–	–	–	–	–
Ploy-24														0	0	–	–	–	–	–
Ploy-23														0	0	–	–	–	–	–
Ploy-22														0	0	–	–	–	–	–
Ploy-21														0	0	–	–	–	–	–
Ploy-20		1												1	1	–	–	–	–	–
Ploy-19														0	0	–	–	–	–	–
Ploy-18														0	0	–	–	–	–	–
Ploy-17														0	0	–	–	–	–	–
Ploy-16					1									1	1	–	–	–	–	–
Ploy-15														0	0	–	–	–	–	–
Ploy-14														0	0	–	–	–	–	–
Ploy-13														0	0	–	–	–	–	–
Ploy-12														0	0	–	–	–	–	–
Ploy-11														0	0	–	–	–	–	–
Ploy-10			1											1	1	–	–	–	–	–
Ploy-09														0	0	–	–	–	–	–
Ploy-08														0	0	–	–	–	–	–
Ploy-07			1											1	1	–	–	–	–	–
Ploy-06														0	0	–	–	–	–	–
Ploy-05		2									1			3	2	–	–	–	–	–
Ploy-04														0	0	–	–	–	–	–
Ploy-03														0	0	–	–	–	–	–
Ploy-02														0	0	–	–	–	–	–
Ploy-01														0	0	–	–	–	–	–
Oyambre 1				2	1	16	44		47	44		28	4	315	32	98.8	1.2	0.9	4.4	94,7
Ploy-00				14	1		1	1	1	255		1	23	321	17	98.1	1.9	1.2	6.2	92.6

Table 4. Summary of quartz OSL and feldspar pIRIR results.

Lab. Code	Sample	Site	Depth,	w.c.	pIRIR D_e,	(n_r)	(n_a)	OSL D_e,	%sat	(n_s)	(n_r)	(n_a)	feldspar dose rate,	quartz dose rate,	pIRIR age,	OSL age,
			cm	%	Gy			Gy					Gy/ka	Gy/ka	ka	ka
12 22 57	Ployambre Duna	Playa Oyambre	50	4	17 ± 2	1	5	0.082 ± 0.005		0	2	21	2.00 ± 0.09	1.08 ± 0.06	8.4 ± 1.0	0.076 ± 0.007
12 22 58	Ployambre 0	Playa Oyambre	10	21	14 ± 4	0	6	0.055 ± 0.002		0	3	21	1.51 ± 0.07	0.59 ± 0.02	9.2 ± 2.4	0.093 ± 0.005
12 22 59	Ployambre 1	Playa Oyambre	1265	20	951 ± 76	0	3	>250	13	3	3	21	2.37 ± 0.10	1.45 ± 0.07	394 ± 36	>170
12 22 60	Ployambre 2	Playa Oyambre	1251	20	929 ± 88	0	3	>175	25	6	6	18	2.22 ± 0.09	1.31 ± 0.06	411 ± 43	>130
12 22 61	Ployambre 3	Playa Oyambre	1226	20	811 ± 66	0	3	>200	44	8	8	10	2.40 ± 0.10	1.48 ± 0.07	331 ± 31	>133
12 22 62	Ployambre 4	Playa Oyambre	1208	20	1127 ± 179	0	3	>190	46	11	14	10	2.49 ± 0.10	1.57 ± 0.08	447 ± 74	>120
12 22 63	Ployambre 5	Playa Oyambre	1193	19	405 ± 40	0	6	>190	37	11	12	18	1.65 ± 0.07	0.73 ± 0.04	236 ± 26	>260
12 22 64	Ployambre 6	Playa Oyambre	1151	12	372 ± 40	0	3	133 ± 5	4	1	2	22	1.94 ± 0.08	1.02 ± 0.05	184 ± 22	**131 ± 9**
12 22 65	Ployambre 7	Playa Oyambre	1107	12	381 ± 17	0	6	>190	32	8	8	17	2.14 ± 0.09	1.23 ± 0.06	170 ± 11	>160
12 22 66	Ployambre 8	Playa Oyambre	1089	20	476 ± 37	0	3	>230	88	21	21	3	3.48 ± 0.14	2.56 ± 0.13	132 ± 12	>90
12 22 67	Ployambre 9	Playa Oyambre	1049	22	526 ± 34	0	3	>190	33	7	7	14	2.81 ± 0.11	1.89 ± 0.09	182 ± 14	>100
12 22 68	Ployambre 10	Playa Oyambre	997	20	N.A.	0	0	>300	74	20	20	7	N.A.	3.25 ± 0.16	N.A.	>90
12 22 69	Ployambre 11	Playa Oyambre	953	13	138 ± 5	0	3	60.4 ± 2.5		0	1	35	1.52 ± 0.07	0.60 ± 0.03	81 ± 5	**101 ± 7**
12 22 70	Ployambre 12	Playa Oyambre	942	19	148 ± 8	0	3	62.3 ± 2.0		0	5	37	1.47 ± 0.07	0.55 ± 0.03	90 ± 7	**113 ± 7**
12 22 71	Ployambre 13	Playa Oyambre	901	18	140 ± 11	0	3	57.7 ± 2.0		0	2	34	1.29 ± 0.07	0.37 ± 0.02	96 ± 10	**155 ± 10**
12 22 72	Ployambre 14	Playa Oyambre	878	18	160 ± 7	0	3	117 ± 6		0	1	26	1.78 ± 0.08	0.86 ± 0.04	82 ± 5	**136 ± 10**
12 22 73	Ployambre 15	Playa Oyambre	845	17	193 ± 4	0	3	88.2 ± 2.5		0	1	23	1.65 ± 0.07	0.73 ± 0.04	108 ± 5	**121 ± 7**
12 22 74	Ployambre 16	Playa Oyambre	811	13	163 ± 5	0	6	66.8 ± 2.4		0	1	23	1.50 ± 0.07	0.58 ± 0.03	98 ± 6	**115 ± 7**
12 22 75	Ployambre 17	Playa Oyambre	775	13	171 ± 3	0	3	88.5 ± 3.4		0	0	24	1.58 ± 0.07	0.67 ± 0.03	98 ± 5	**133 ± 9**
12 22 76	Ployambre 18	Playa Oyambre	727	13	207 ± 12	0	3	147 ± 9		0	1	27	2.01 ± 0.08	1.09 ± 0.05	95 ± 7	**135 ± 11**
12 22 77	Ployambre 19	Playa Oyambre	698	22	329 ± 33	0	3	>190	36	12	13	20	3.21 ± 0.13	2.29 ± 0.11	98 ± 11	>83

(*Continued*)

Table 4. (*Continued*)

Lab. Code			Sample	Site	Depth,	w.c.	pIRIR D_e,	(n_r)	(n_a)	OSL D_e,	%sat	(n_s)	(n_r)	(n_a)	feldspar dose rate,	quartz dose rate,	pIRIR age,	OSL age,
12	22	78	Ployambre 20	Playa Oyambre	677	15	239 ± 19	0	3	96.4 ± 3.5		0	1	35	1.62 ± 0.07	0.70 ± 0.03	138 ± 13	**137 ± 9**
12	22	79	Ployambre 21	Playa Oyambre	640	14	330 ± 63	0	3	136 ± 6		0	0	27	1.90 ± 0.08	0.98 ± 0.05	166 ± 34	**139 ± 10**
12	22	80	Ployambre 22	Playa Oyambre	607	15	371 ± 72	0	3	124 ± 7		0	1	21	1.77 ± 0.08	0.85 ± 0.04	201 ± 41	**146 ± 12**
12	22	81	Ployambre 23	Playa Oyambre	564	12	208 ± 22	0	3	94 ± 4		0	2	28	1.80 ± 0.08	0.88 ± 0.04	107 ± 13	**107 ± 7**
12	22	82	Ployambre 24	Playa Oyambre	521	11	246 ± 28	0	3	112 ± 5		0	1	23	1.98 ± 0.08	1.06 ± 0.05	117 ± 15	**105 ± 8**
12	22	83	Ployambre 25	Playa Oyambre	493	11	213 ± 10	0	3	114 ± 5		0	1	23	1.99 ± 0.08	1.07 ± 0.05	99 ± 7	**106 ± 7**
12	22	84	Ployambre 26	Playa Oyambre	448	12	155 ± 5	0	3	71.0 ± 3.4		0	3	21	1.71 ± 0.07	0.79 ± 0.04	82 ± 5	**90 ± 6**
12	22	85	Ployambre 27	Playa Oyambre	392	8	152 ± 5	0	3	59.7 ± 2.2		0	3	29	1.54 ± 0.07	0.62 ± 0.03	89 ± 5	**97 ± 6**
12	22	86	Ployambre 28	Playa Oyambre	362	8	144 ± 6	0	3	81.3 ± 3.7		0	3	21	1.69 ± 0.07	0.77 ± 0.04	76 ± 5	**105 ± 7**
12	22	87	Ployambre 29	Playa Oyambre	328	8	163 ± 6	0	3	70.9 ± 4.2		0	1	23	1.72 ± 0.08	0.80 ± 0.04	86 ± 5	**88 ± 7**
12	22	88	Ployambre 30	Playa Oyambre	295	8	164 ± 7	0	3	77.7 ± 4.0		0	0	18	1.77 ± 0.08	0.85 ± 0.04	84 ± 5	**91 ± 7**
12	22	89	Ployambre 31	Playa Oyambre	273	9	168 ± 7	0	3	83.8 ± 3.7		0	1	26	1.94 ± 0.08	1.02 ± 0.05	79 ± 5	**82 ± 6**
12	22	90	Ployambre 32	Playa Oyambre	230	8	184 ± 27	0	3	62.5 ± 3.5		0	0	21	1.49 ± 0.07	0.57 ± 0.03	113 ± 19	**110 ± 8**
12	22	91	Ployambre 33	Playa Oyambre	201	8	171 ± 8	0	3	92.2 ± 6.3		0	2	22	1.83 ± 0.08	0.92 ± 0.04	85 ± 6	**101 ± 9**
12	22	92	Ployambre 34	Playa Oyambre	147	8	200 ± 4	0	6	113 ± 5		0	0	18	2.16 ± 0.09	1.24 ± 0.06	85 ± 4	**91 ± 7**
12	22	93	Ployambre 35	Playa Oyambre	110	8	165 ± 4	0	3	79.2 ± 3.5		0	0	18	1.62 ± 0.07	0.70 ± 0.03	92 ± 5	**113 ± 8**
12	22	94	Ployambre 36	Playa Oyambre	47	8	170 ± 8	0	3	85.1 ± 2.7		0	3	30	2.17 ± 0.09	1.25 ± 0.06	71 ± 5	**68 ± 4**

w.c. – estimated time-averaged water content of the samples during burial. (nr) – number of rejected aliquots, (na) – number of accepted aliquots, (ns) – number of rejected aliquots due to saturation. Uncertainties (1σ) on the ages incorporate both systematic and random components. N.A. – not available, no K-feldspar grains could be extracted. Before calculating the feldspar pIRIR ages of samples 122259–94, a residual dose of 15 ± 1 Gy was subtracted from the D_e values based on the results from the modern analogue samples. Ages in bold were used for interpretation.

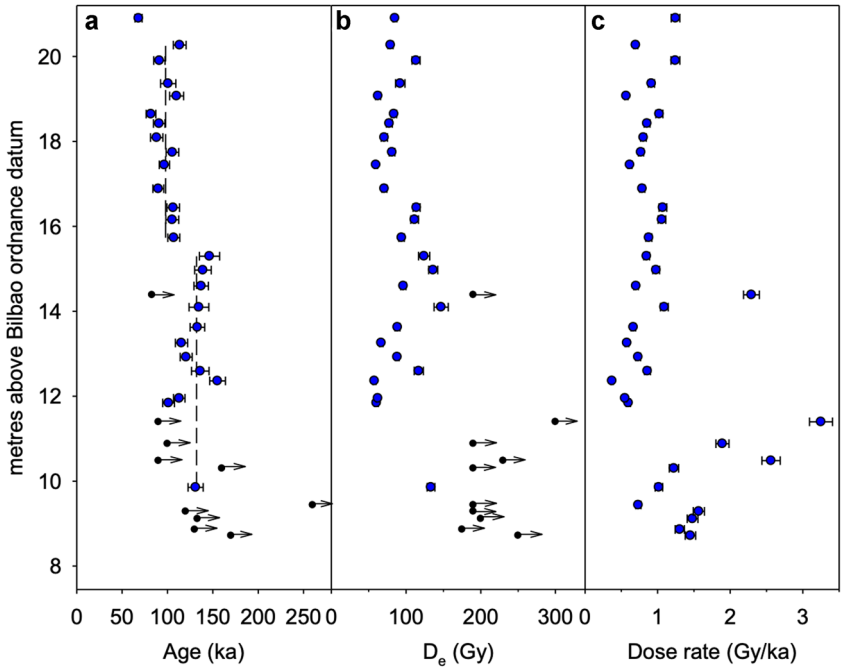

Figure 6. Quartz OSL ages (a), equivalent doses (b) and total dose rates (c) plotted according to their topographic height (m a.B.o.d.). Samples that are considered saturated (too many aliquots with natural quartz OSL signal above or in saturation on the dose response curve) have their D_e and age shown as minimum ages/doses (black circles with arrow). Quartz OSL ages and D_e values that are considered reliable are shown as blue symbols. The vertical dashed lines are drawn at 132 and 98 ka for the bottom and top part of the section, respectively. Uncertainties (1σ) only contain random components. [Color figure can be viewed at wileyonlinelibrary.com]

Additionally, Pérez-Díaz *et al.* (2017) analysed the pollen contents of 14 different silty samples interbedded in the general sandy sequence of unit 2 [from layers 5 (three replicates), 9, 10, 11, 15 (two replicates), 16 (two replicates), 18, 24, 25 and 26] and identified some climate variability during this interval. Cold conditions in the lower (layers 5–9) and upper (layers 24–26) parts were characterized by large coniferous forests of *Pinus* and *Abies*, with *Betula*, *Alnus* and Poaceae in a secondary role. More temperate conditions in the middle (layers 10–18) were suggested by the dominance of deciduous forests with *Quercus* and *Corylus*, together with the presence of some relict taxa such as *Fagus* and *Carpinus*.

Luminescence dating

Four samples were taken in pebbly fine sands representing a beach environment, Ploy-01 to Ploy-04 (NLL lab codes 122259–122262); 32 samples located above, representing aeolian and palustrine environments, Ploy-05 to Ploy-36 (NLL lab codes 122263–122294) (Table 4), and two modern analogues of aeolian dune and beach sands, Ploy-dune and Ploy-00 (NLL lab codes 122257 and 122258).

The results of quartz OSL and feldspar pIRIR dating are presented in Table 4. Luminescence characteristics (e.g. dose response curve, recycling ratio, preheat plateau, dose recovery) of quartz and feldspar and the radionuclide concentrations are given in the Supporting Information.

Discussion

Age of the coastal terrace sequence

The two modern analogue samples (122257 and 58) give quartz D_e values of 60–80 mGy (equivalent to <100 years old) indicating that in this environment incomplete bleaching of the quartz OSL signal is not likely to be of concern when D_e values >50 Gy are measured. Furthermore, a comparison of the quartz OSL ages with the feldspar pIRIR$_{200,290}$ ages, the latter obtained using a much harder-to-bleach signal, strongly suggests that the quartz OSL signals from these samples were well-bleached at deposition (Table 4) (Murray *et al.*, 2012).

Figure 6 shows the quartz OSL data plotted as function of the topographic height of the samples (m a.B.o.d.). It can be seen that both the D_e and dose rate vary significantly down the section but that the scatter in age as a function of depth is considerably reduced (albeit still over-dispersed towards the bottom of the section). It is well known that the reliability of quartz OSL dating using the fast component is not guaranteed when D_e values greater than ~150 Gy are measured (e.g. Buylaert *et al.*, 2007; Chapot *et al.*, 2012; Timar-Gabor and Wintle, 2013), as the natural OSL signals approach the saturation level of the dose response curves. The measured

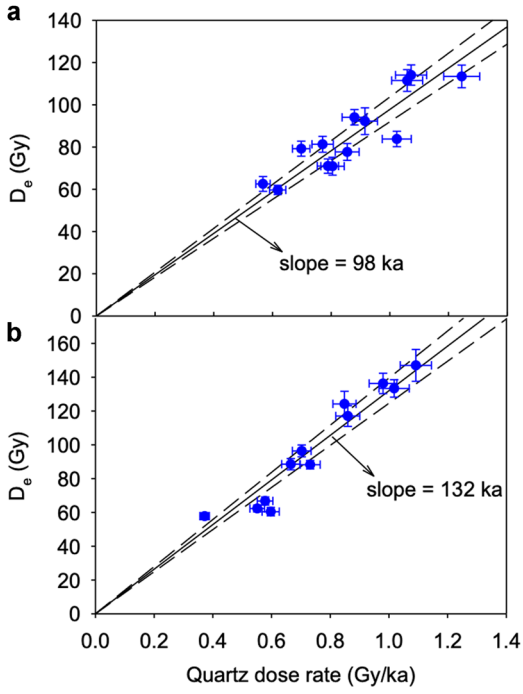

Figure 7. Quartz OSL D_e as a function of total dose rate for the upper (a) and lower (b) part of the section. Only samples that do not suffer from saturation effects were used to construct these isochrones. Dashed lines show the 95% confidence intervals. Uncertainties (1σ) comprise random components only. [Color figure can be viewed at wileyonlinelibrary.com]

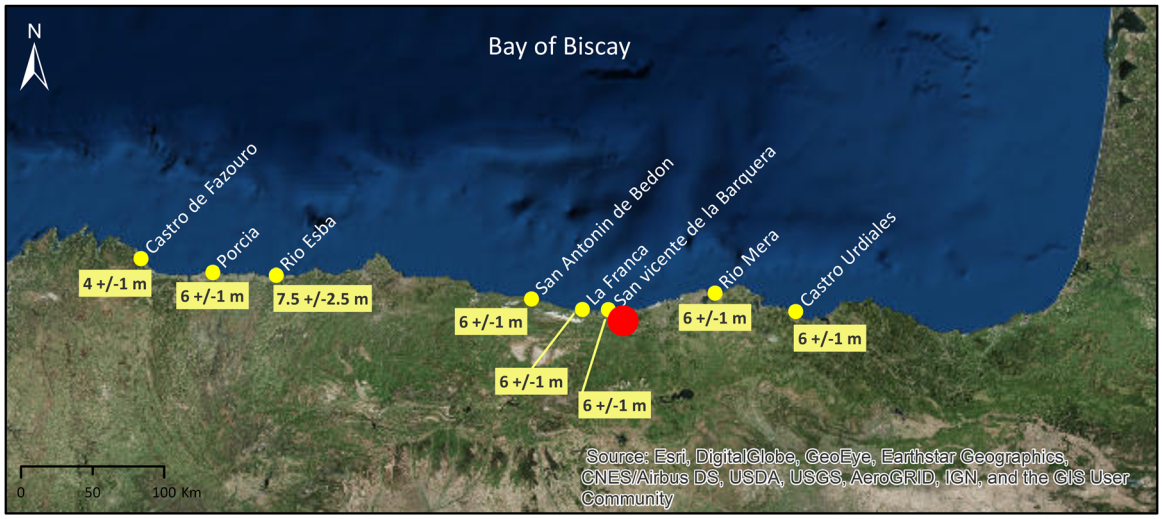

Figure 8. Maximum sea-level elevation during the Last Interglacial along the Cantabrian coast presented by Pedoja *et al.* (2018). The study site of Oyambre is represented as a red dot. Satellite image from Esri Basemap Gallery. [Color figure can be viewed at wileyonlinelibrary.com]

quartz OSL dose response curves of this material are quite variable even within the same sample (see Supporting Information). For 26 samples (122294–78, 76–69 and 64) the natural signals lie well below the saturation level of the dose response curve and the D_e estimates are considered reliable (blue symbols in Fig. 6a,b). The remaining 10 samples showed a significant number of aliquots (13–88% of the total number of aliquots measured) for which the natural signal lay in the saturation level of the dose response curve (either above laboratory saturation, or interpolation was deemed unreliable due to no or very limited luminescence growth as a function of dose). For these samples, only minimum D_e values are given (black symbols with arrow in Fig. 6a,b; greater than the values in Table 4). Only quartz ages that do not suffer from saturation effects were used for interpretation (bold ages in Table 4 and blue symbols in Fig. 6a). For some samples (e.g. 122277, 68–66), quartz is saturated due to locally higher dose rates and for other samples (122262–59, collected from layers 2 and 3) this could be because the layers are older than MIS 5 or because of very fast erosion/deposition of grains (without significant bleaching of quartz) sourced from the soft cliff (Oligocene marls). However, the most probable stratigraphic interpretation is that layers 1–3 (beach deposits) correspond to the transgressive system of MIS 5, overlaid by layer 4 (aeolian sand) which is dated as 131 ± 9 ka.

Two periods of rapid deposition can be deduced from the quartz OSL ages. A first period of rapid deposition occurred at ~130 ka (layers 4–12); this age is consistent with the onset of MIS 5e (e.g. Cuffey and Marshall, 2000). A second period of rapid deposition occurs at ~100 ka (layers 13–24), consistent with MIS 5c. Because of the variability in dose rate (and thus D_e) of these samples, we can construct isochrones for these two sets of samples (Fig. 7); this is further evidence that the quartz OSL signal was well bleached at deposition and meaningful D_e values are measured. The top of the section (layer 26) is dated to ~70 ka (sample 122294). It appears that the peaks of the glacial sub-stages MIS 5d (~109 ka) and MIS 5b (~87 ka) are not recorded by these sedimentary deposits.

MIS 5e sea-level highstand

Current consensus on global MSL during the LIG is 5–9 m above modern (Dutton *et al.*, 2015). Integrating previous observations from the literature with the outputs of GIA models, Kopp *et al.* (2009) found (95% probability) that global MSL at MIS 5e reached 6.6 m above current sea level. Murray-Wallace and Woodroffe (2014), analysing a considerable amount of literature, proposed that MIS 5e sea-level highstand was 6 ± 4 m higher than modern MSL. Values in the range of 6–9 m above present were derived from global compilations of RSL data combined with GIA modelling (Dutton *et al.*, 2015). Düsterhus *et al.* (2016), with a different statistical approach, obtained a median estimate of 7.5 ± 1.1 m but acknowledged a strong sensitivity to the assumptions made in the analysis. In our location, a local deviation from these ranges could be expected, given that the Oyambre record represents an RSL highstand.

With regards to the age of the LIG coastal deposits, Pedoja *et al.* (2011) compiled a large number of palaeoshoreline sequences around the world with the aim of assessing vertical land motion. They gathered information of 890 MIS 5e deposits with ages ranging from 128 ± 1 to 116 ± 1 ka. Dutton *et al.* (2015) considered MIS 5e to be between 129 and 116 ka and concluded that most studies suggest that peak global MSL occurred in the range of 122–119 ka. A study of coastal sediments in Brittany (France), in a stratigraphic position corresponding to the end of MIS 5e, obtained a probable age of 103 ± 17 ka using thermoluminescence dating (Loyer *et al.*, 1995), while Murray and Funder (2003) obtained an expected age range of 133–125 ka in Denmark. In the western coast of Iberia (Figueira da Foz, western central Portugal), Ramos *et al.* (2012) dated an MIS 5 coastal terrace, providing a quartz OSL age of 126 ± 9 ka from a marine stratigraphic level at an elevation of 7.4–9.6 m above MSL. Pedoja *et al.* (2018), expanding previous works (Pedoja *et al.*, 2011, 2014), presented an updated database of maximum elevation in a large number of sites in Europe, and several in the Cantabrian coast, close to our study area (Fig. 8). According to these stratigraphic and sedimentological data, sea-level highstand in the Cantabrian coast during MIS 5e ranged from 4 ± 1 m in Castro de Fazouro to 7.5 ± 2.5 m in Río Esba, even though in six of the sites, including those closer to Oyambre, the estimated maximum elevation was 6 ± 1 m.

Conclusions

The coastal terrace preserved at the Oyambre beach (northern Spain) is 15.3 m thick and has a basal marine transgressive surface (palaeowave-cut surface on Oligocene sandy marls) at an elevation of 4.50 m above regional MSL. The lower part of

the Pleistocene sedimentary succession (unit 1, layers 1–3), comprising well-sorted and rounded gravels and pebbly sands, is interpreted as beach deposits. Its upper part (unit 2), consisting of layers of medium to fine sands intercalated by thinner mud layers, is interpreted as aeolian and palustrine deposits. Luminescence dating shows that the sedimentary succession (unit 2) indeed represents the Last Interglacial period. Furthermore, two periods of rapid deposition can most likely be distinguished, one at ~130 ka (MIS 5e) and another at ~100 ka (MIS 5c). The dating indicates that the peaks of the glacial sub-stages MIS 5d (~109 ka) and MIS 5b (~87 ka) are not recorded by the sedimentary deposits.

The MIS 5e marine maximum flooding surface should be represented by the boundary between layers 3 and 4, at an elevation of 6.85 m above present MSL. This precise elevation for the MIS 5e.

Acknowledgements. This work was co-funded by projects Ministerio de Economía y Competitividad – MINECO (CGL2013-41083-P and RTI2018-095678-B-C21, MCIU/AEI/FEDER UE), Euskal Herriko Unibertsitatea – UPV/EHU (UFI11/09), Eusko Jaurlaritza – EJ GV–1 (IT365-10, IT767-13 and IT976-16) and Fundação Para a Ciência e Tecnologia, with FEDER and COMPETE 2020 funds, through project UID/MAR/04292/2020 – MARE (Marine and Environmental Sciences Centre). Susi Fernández (Mendi Topografia, Spain) determined the topographic location of the samples. The Geology Group of the University of Cantabria (A. Cendrero, J. R. Diaz de Terán, J. Remondo and V. Bruschi) suggested the scientific interest of the Oyambre deposit to the authors. Manu Monge-Ganuzas and Eduardo Leorri assisted in the field. Haizea Quintas revised the foraminiferal samples. Dr Natasha Barlow and another anonymous reviewer greatly improved the original manuscript with their comments and constructive suggestions. This is contribution 44 of the Geo-Q Zentroa Research Unit (Joaquín Gómez de Llarena Laboratory). J.-P. Buylaert received funding from the European Research Council under the European Union Horizon 2020 research and innovation programme ERC-2014-StG 639904 – RELOS.

Declaration of interest

The authors declare that they hold no competing financial or non-financial interests.

Data availability statement

The data supporting the findings of this study are available within the article and its Supporting Information. Any additional data are available from the authors upon request.

Supporting information

Additional supporting information can be found in the online version of this article.This article includes online-only Supplemental Data.

Section 1. Geographical location of tube samples for luminescence dating taken at the Oyambre outcrop.

Section 2. Luminescence characteristics of quartz and feldspar at the Oyambre outcrop.

Figure S1. First 10 seconds of quartz OSL decay curves for sample 122265 and calibration quartz (batch 122) measured using blue-light stimulation (~80 mW cm^{-2}). Signals were normalized to the first datapoint. It can be seen that quartz from the Oyambre sequence is dominated by a fast component.

Figure S2. Dose response curves for two quartz aliquots from sample 122265 fitted with single saturation exponential function. The dose response curve of one aliquot (filled symbols) has a relatively high characteristic dose (~103 Gy) allowing interpolation up to ~200 Gy. The other aliquot (open symbols) saturates much earlier (characteristic dose ~60 Gy) and interpolation on the dose response curve is not possible.

Figure S3a. Quartz SAR OSL preheat plateau data for sample 122292. The cut-heat temperature was always 40 °C lower than the preheat temperature, except for preheats 160–200 for which it was always 160 °C. At least three aliquots were measured at each dose point; average (± SE) shown as solid and dashed lines. Bottom graph shows corresponding recycling ratios and a solid line drawn at unity to serve as eye guide.

Figure S3b. Quartz SAR OSL preheat plateau data for sample 122270. The cut-heat temperature was always 40 °C lower than the preheat temperature, except for preheats 160–200 for which it was always 160 °C. At least three aliquots were measured at each dose point; average (± SE) shown as solid and dashed lines. Bottom graph shows corresponding recycling ratios and a solid line drawn at unity to serve as eye guide.

Figure S4. Histograms summarizing recycling ratios (a) and OSL IR depletion ratios (b) for 16 samples (122264, 71–73, 75–78, 81–83, 86–89 and 94) from the Oyambre section. At least six aliquots were measured per sample.

Figure S5. Histograms summarizing dose recovery ratios for 31 samples Three aliquots were measured per sample. One outlier (ratio 1.90) was removed from the histogram. Given dose = 109 Gy.

Figure S6. Feldspar pIRIR versus quartz OSL age plot.

Table S1. Geographical location of tube samples for luminescence dating taken at the Oyambre outcrop. Topographic positions are shown in metres above Bilbao ordnance datum (corresponding to 2.40 m below Bilbao MSL).

Table S2. Radionuclide concentrations and dry beta and gamma dose rates.

Abbreviations. a.B.o.d., above Bilbao ordnance datum; GIA, glacial isostatic adjustment; GPS-RTK, Global Positioning System-Real Time Kinematic; LIG, Last Interglacial Stage; MIS, Marine Oxygen Isotope Stage; MSL, mean sea level; OSL, optically stimulated luminescence; pIRIR, post-infrared infrared; RSL, relative sea level; SAR, single aliquot regeneration; SLR, sea level rise.

References

Aitken MJ. 1998. *An Introduction to Optical Dating. The Dating of QuaternaryQ Sediments by the Use of Photon-Stimulated Luminescence*. Oxford University Press: Oxford.

Alonso A, Pagés JL. 2007. Stratigraphy of Late Pleistocene coastal deposits in Northern Spain. *Journal of Iberian Geology* **33**: 207–220.

Barlow NLM, McClymont EL, Whitehouse PL *et al*. 2018. Lack of evidence for a substantial sea-level fluctuation within the Last Interglacial. *Nature Geoscience* **11**: 627–634.

Buylaert J-P, Jain M, Murray AS *et al*. 2012. A robust feldspar luminescence dating method for Middle and Late Pleistocene sediments. *Boreas* **41**: 435–451.

Buylaert JP, Vandenberghe D, Murray AS *et al*. 2007. Luminescence dating of old (>70 ka) Chinese loess: a comparison of single-aliquot OSL and IRSL techniques. *Quaternary Geochronology* **2**: 9–14.

Candy I, Schreve DC, Sherriff J *et al*. 2014. Marine Isotope Stage 11: palaeoclimates, palaeoenvironments and its role as an analogue for the current interglacial. *Earth-Science Reviews* **128**: 18–51.

Chapot MS, Roberts HM, Duller GAT *et al*. 2012. A comparison of natural- and laboratory-generated dose response curves for quartz optically stimulated luminescence signals from Chinese Loess. *Radiation Measurements* **47**: 1045–1052.

Creveling JR, Mitrovica JX, Clark PU *et al*. 2017. Predicted bounds on peak global mean sea level during marine isotope stages 5a and 5c. *Quaternary Science Reviews* **163**: 193–208.

Cuffey KM, Marshall SJ. 2000. Substantial contribution to sea-level rise during the last interglacial from the Greenland ice sheet. *Nature* **404**: 591–594.

Cunha PP, Martins AA, Buylaert J-P *et al*. 2019. The lowermost Tejo river terrace at Foz do Enxarrique, Portugal: a palaeoenvironmental archive from c. 60–35 ka and its implications for the last Neanderthals in Westernmost Iberia. *Quaternary* **2**: 3.

Cunha PP, Martins AA, Huot S *et al*. 2008. Dating the Tejo river lower terraces in the Ródão area (Portugal) to assess the role of tectonics and uplift. *Geomorphology* **102**: 43–54.

Duller GAT. 2008. *Luminescence Dating: Guidelines on Using Luminescence Dating in Archaeology*. English Heritage: Swindon.

Düsterhus A, Tamisiea ME, Jevrejeva S. 2016. Estimating the sea level highstand during the last interglacial: a probabilistic massive ensemble approach. *Geophysical Journal International* **206**: 900–920.

Dutton A, Carlson AE, Long AJ *et al*. 2015. Sea-level rise due to polar ice-sheet mass loss during past warm periods, *Science*: aaa4019–aaa4019.

Edwards ME, Mock CJ, Finney BP *et al*. 2001. Potential analogues for paleoclimatic variations in eastern interior Alaska during the past 14,000 yr: atmospheric-circulation controls of regional temperature and moisture responses. *Quaternary Science Reviews* **20**: 189–202.

Flor G. 1980. Los carbonatos biogénicos de la zona intermareal de playa en relación con la dinámica y morfología costeras en Asturias y Cantabria. *Boletín de la Real Sociedad Española de Historia Natural. Sección Geológica* **78**: 275–279.

García-Codrón JC, Rasilla, Álvarez DF. 2006. Coastline retreat, sea level variability and atmospheric circulation in Cantabria (Northern Spain). *Journal of Coastal Research* 49–54.

Garzón G, Alonso A, Torres T *et al*. 1996. Edad de las playas colgadas y turberas de Oyambre y Merón (Cantabria). *Geogaceta* **20**: 498–501.

Gilford DM, Ashe EL, DeConto RM *et al*. 2020. Could the last interglacial constrain projections of future Antarctic ice mass loss and sea-level rise? *Journal of Geophysical Research: Earth Surface* **125** e2019.

Goelzer H, Huybrechts P, Loutre M-F *et al*. 2016. Last Interglacial climate and sea-level evolution from a coupled ice sheet–climate model. *Climate of the Past* **12**: 2195–2213.

Guérin G, Mercier N, Adamiec G. 2011. *Dose-rate conversion factors: update. Ancient TL* **29**: 5–8.

Hay CC, Morrow E, Kopp RE, Mitrovica JX. 2015. Probabilistic reanalysis of twentieth-century sea-level rise. *Nature* **517**: 481–484. https://doi.org/10.1038/nature14093

Hearty PJ, Hollin JT, Neumann AC *et al*. 2007. Global sea-level fluctuations during the Last Interglaciation (MIS 5e). *Quaternary Science Reviews* **26**: 2090–2112.

Kopp RE, Simons FJ, Mitrovica JX *et al*. 2009. Probabilistic assessment of sea level during the last interglacial stage. *Nature* **462**: 863–867.

Kopp RE, Simons FJ, Mitrovica JX, Maloof AC, Oppenheimer M. 2013. A probabilistic assessment of sea level variations within the last interglacial stage. *Geophysical Journal International* **193**: 711–716. https://doi.org/10.1093/gji/ggt029

Kukla GJ, Bender ML, de Beaulieu J-L *et al*. 2002. Last interglacial climates. *Quaternary Research* **58**: 2–13.

Lambeck K, Esat TM, Potter E-K. 2002. Links between climate and sea levels for the past three million years. *Nature* **419**: 199–206. https://doi.org/10.1038/nature01089

Lamothe M. 2016. Luminescence dating of interglacial coastal depositional systems: recent developments and future avenues of research. *Quaternary Science Reviews* **146**: 1–27.

López-Fernández C, Llana-Fúnez S, Fernández-Viejo G *et al*. 2020. Comprehensive characterization of elevated coastal platforms in the north Iberian margin: A new template to quantify uplift rates and tectonic patterns. *Geomorphology* **364**: 107242.

Loutre MF, Berger A. 2003. Marine Isotope Stage 11 as an analogue for the present interglacial. *Global and Planetary Change* **36**: 209–217.

Loyer S, Van Vliet-Lanoë B, Monnier JL *et al*. 1995. La coupe de Nantois (Baie de Saint-Brieuc, France): datations par thermoluminescence (TL) et données paléoenvironnementales nouvelles pour le Pléistocène de Bretagne [The Nantois section (Saint-Brieuc Bay France): new thermoluminescence (TL) datings and palaeoenvironnemental data for the Pleistocene of Brittany.]. *Quaternaire* **6**: 21–33.

Mary G. 1971. Les formations quaternaires de la côte Asturienne (Espagne) entre Ribadesella et Camillas. *Bulletin de l'Association française pour l'étude du Quaternaire* **8**: 111–118.

Mary G. 1983. Evolución del margen costero de la Cordillera Cantábrica en Asturias desde el Mioceno. *Trabajos de Geología* **13**: 3–35.

Masson-Delmotte V, Schulz M, Abe-Ouchi A *et al*. 2013. Information from paleoclimate archives. In *Climate Change 2013: The Physical Science Basis. Contribution of Working Group I to the Fifth Assessment Report of the Intergovernmental Panel on Climate Change*, Stocker TF, Qin D, Plattner GK, Tignor M, Allen SK, Boschung J, Nauels A, Xia Y, Bex V, Midgley PM (eds). Cambridge University Press: Cambridge.

Mengaud L. 1920. Recherches géologiques dans la région cantabrique. *Bulletin de la Société d'Histoire Naturelle de Toulouse* **48**: 73–272.

Murray AS, Funder S. 2003. Optically stimulated luminescence dating of a Danish Eemian coastal marine deposit: a test of accuracy. *Quaternary Science Reviews* **22**: 1177–1183.

Murray AS, Helsted LM, Autzen M *et al*. 2018. Measurement of natural radioactivity: calibration and performance of a high-resolution gamma spectrometry facility. *Radiation Measurements* **120**: 215–220.

Murray AS, Svendsen JI, Mangerud J, Astakhov VI. 2007. Testing the accuracy of quartz OSL dating using a known-age Eemian site on the river Sula, northern Russia. *Quaternary Geochronology* **2**: 102–109. https://doi.org/10.1016/j.quageo.2006.04.004

Murray AS, Thomsen KJ, Masuda N *et al*. 2012. Identifying well-bleached quartz using the different bleaching rates of quartz and feldspar luminescence signals. *Radiation Measurements* **47**: 688–695.

Murray AS, Wintle AG. 2003. The single aliquot regenerative dose protocol: potential for improvements in reliability. *Radiation Measurements* **37**: 377–381.

Murray J. 1979. British nearshore foraminiferids. *Synopses of the British Fauna* **16** 1–68.

Murray-Wallace CV, Woodroffe CD. 2014. *Quaternary Sea-Level Changes: a Global Perspective*. Cambridge University Press: Cambridge.

Oldfield F. 2005. *Environmental Change: Key Issues and Alternative Perspectives*. Cambridge University Press: Cambridge.

Oppenheimer M, Glavovic BC, Hinkel J, Wal R, van de, Magnan AK, Abd-Elgawad A, Cai R, CifuentesJara M, DeConto RM, Ghosh T, Hay J, Isla F, Marzeion B, Meyssignac B, Sebesvari Z, 2019. Sea Level Rise and Implications for Low-Lying Islands, Coasts and Communities. In: Pörtner HO, Roberts DC, Masson-Delmotte V, Zhai P, Tignor M, Mintenbeck K, Nicolai M, Okem A, Petzold J, Rama B, Weyer N. (Eds). IPCC Special Report on the Ocean and Cryosphere in a Changing Climate. In press.

Payros A, Dinarès-Turell J, Monechi S *et al*. 2015. The Lutetian/Bartonian transition (Middle Eocene) at the Oyambre section (northern Spain): implications for standard chronostratigraphy. *Palaeogeography, Palaeoclimatology, Palaeoecology* **440**: 234–248.

Pedoja K, Husson L, Johnson ME *et al*. 2014. Coastal staircase sequences reflecting sea-level oscillations and tectonic uplift during the Quaternary and Neogene. *Earth-Science Reviews* **132**: 13–38.

Pedoja K, Husson L, Regard V *et al*. 2011. Relative sea-level fall since the last interglacial stage: are coasts uplifting worldwide? *Earth-Science Reviews* **108**: 1–15.

Pedoja K, Jara-Muñoz J, De Gelder G *et al*. 2018. Neogene–Quaternary slow coastal uplift of Western Europe through the perspective of sequences of strandlines from the Cotentin Peninsula (Normandy, France). *Geomorphology* **303**: 338–356.

Pérez-Díaz S, Cearreta A, López-Sáez JA *et al*. 2017. Vegetation dynamics and climate variability during the MIS-5 in the northern Iberian coast: the palynological study of the Oyambre deposit. In *Abstract Book. Presented at the PAGES Zaragoza 2017 5th Open Science Meeting, Global Challenges for our Common Future: a paleoscience perspective, Instituto Pirenaico de Ecología, Zaragoza*; 341.

Prescott JR, Hutton JT. 1994. Cosmic ray contributions to dose rates for luminescence and ESR dating: large depths and long-term time variations. *Radiation Measurements* **23**: 497–500.

Ramos AM, Cunha PP, Cunha LS *et al*. 2012. The River Mondego terraces at the Figueira da Foz coastal area (western central Portugal): geomorphological and sedimentological characterization of a terrace staircase affected by differential uplift and glacio-eustasy. *Geomorphology* **165–166**: 107–123.

Revi A, Satterthwhite DE, Aragón-Durand F *et al*. 2014. Urban areas. In *Climate Change 2014: Impacts, Adaptation, and Vulnerability. Part A Global and Sectoral Aspects. Contribution of Working Group II to the Fifth Assessment Report of the Intergovernmental Panel on Climate Change*, Field CB, Barros VR, Dokken DJ, Mach KJ, Mastrandrea MD, Bilir TE, Chatterjee M, Ebi KL, Estrada YO, Genova RC, Girma B, Kissel ES, Levy AN, MacCracken S, Mastrandea PR, White LL (eds). Cambridge University Press: Cambridge; 535–612.

Rohling EJ, Grant K, Hemleben C *et al*. 2008. High rates of sea-level rise during the last interglacial period. *Nature Geoscience* **1**: 38–42.

Sainz de Murieta E 2016. *Environmental and economic impact of sea-level rise on the Basque Coast*. PhD Dissertation, University of the Basque Country UPV/EHU.

Stevens T, Buylaert JP, Thiel C *et al*. 2018. Ice-volume-forced erosion of the Chinese Loess Plateau global Quaternary stratotype site. *Nature Communications* **9**: 983.

Stirling CH, Esat TM, Lambeck K *et al*. 1998. Timing and duration of the Last Interglacial: evidence for a restricted interval of widespread coral reef growth. *Earth and Planetary Science Letters* **160**: 745–762.

Timar-Gabor A, Wintle AG. 2013. On natural and laboratory generated dose response curves for quartz of different grain sizes from Romanian loess. *Quaternary Geochronology* **18**: 34–40.

Tzedakis C. 2003. Timing and duration of Last Interglacial conditions in Europe: a chronicle of a changing chronology. *Quaternary Science Reviews* **22**: 763–768.

Tzedakis PC. 2010. The MIS 11 – MIS 1 analogy, southern European vegetation, atmospheric methane and the "early anthropogenic hypothesis". *Climate of the Past* **6**: 131–144.

Vandenberghe D, De Corte F, Buylaert J-P, Kučera J, Van den haute P. 2008. On the internal radioactivity in quartz. *Radiation Measurements, Proceedings of the 15th Solid State Dosimetry (SSD15)* **43**: 771–775. https://doi.org/10.1016/j.radmeas.2008.01.016

Wintle AG, Murray AS. 2000. Quartz OSL: effects of thermal treatment and their relevance to laboratory dating procedures. *Radiation Measurements* **32**: 387–400.

Yin Q, Berger A. 2015. Interglacial analogues of the Holocene and its natural near future. *Quaternary Science Reviews* **120**: 28–46.

